
This copy is for your personal, non-commercial use only.

If you wish to distribute this article to others, you can order high-quality copies for your colleagues, clients, or customers by [clicking here](#).

Permission to republish or repurpose articles or portions of articles can be obtained by following the guidelines [here](#).

The following resources related to this article are available online at www.sciencemag.org (this information is current as of November 14, 2011):

Updated information and services, including high-resolution figures, can be found in the online version of this article at:

<http://www.sciencemag.org/content/334/6052/75.full.html>

Supporting Online Material can be found at:

<http://www.sciencemag.org/content/suppl/2011/09/07/science.1209150.DC1.html>

<http://www.sciencemag.org/content/suppl/2011/09/08/science.1209150.DC2.html>

A list of selected additional articles on the Science Web sites **related to this article** can be found at:

<http://www.sciencemag.org/content/334/6052/75.full.html#related>

This article appears in the following **subject collections**:

Materials Science

http://www.sciencemag.org/cgi/collection/mat_sci

(*p*-xylene from *o*-xylene) with a *p*-xylene/*o*-xylene separation factor of 40 to 70 and *p*-xylene permeance of 3×10^{-7} mol m⁻²s⁻¹ Pa⁻¹ at 150°C (fig. S11). Preliminary findings from MWW nanosheet coatings show that a seed layer of similar quality to that of MFI nanosheets can be obtained (fig. S12A), which, after secondary growth (fig. S12B), leads to membranes exhibiting molecular sieving properties (fig. S12, C and D) with ideal selectivities for He/H₂ and He/N₂ up to 3 and 17, respectively, which are different from the values expected from Knudsen diffusion and consistent with the small transport-limited aperture of MWW along the *c* axis.

These findings indicate that the films fabricated using exfoliated zeolite nanosheets exhibit the expected molecular sieving properties and are appropriate to be used as membranes. The exfoliation and purification process described here may also be applicable to other microporous layered materials to obtain high-aspect-ratio crystalline nanosheets with high purity and uniformity of thickness. Moreover, the simple film formation method introduced, based only on filtration of the nanosheet suspensions, is likely to be easily scalable for large-scale membrane formation on low-cost, commercially available porous supports with large pores and rough surfaces.

References and Notes

- M. E. Leonowicz, J. A. Lawton, S. L. Lawton, M. K. Rubin, *Science* **264**, 1910 (1994).

- A. Corma, V. Fornes, S. B. Pergher, T. L. M. Maesen, J. G. Buglass, *Nature* **396**, 353 (1998).
- M. Choi *et al.*, *Nature* **461**, 246 (2009).
- M. A. Snyder, M. Tsapatsis, *Angew. Chem. Int. Ed.* **46**, 7560 (2007).
- M. E. Davis, *Nature* **417**, 813 (2002).
- C. M. Lew, R. Cai, Y. S. Yan, *Acc. Chem. Res.* **43**, 210 (2010).
- V. V. Narkhede, H. Gies, *Chem. Mater.* **21**, 4339 (2009).
- N. Takahashi, H. Hata, K. Kuroda, *Chem. Mater.* **23**, 266 (2011).
- J. H. Yu, R. R. Xu, *Acc. Chem. Res.* **36**, 481 (2003).
- Q. M. Gao *et al.*, *J. Solid State Chem.* **129**, 37 (1997).
- H. M. Yuan *et al.*, *J. Solid State Chem.* **151**, 145 (2000).
- Z. Li, B. Marler, H. Gies, *Chem. Mater.* **20**, 1896 (2008).
- G. G. Juttu, R. F. Lobo, *Microporous Mesoporous Mater.* **40**, 9 (2000).
- I. Ogino *et al.*, *J. Am. Chem. Soc.* **133**, 3288 (2011).
- L. Liu *et al.*, *Inorg. Chem.* **48**, 4598 (2009).
- C. Rubio *et al.*, *Eur. J. Inorg. Chem.* **2010**, 159 (2010).
- W. J. Roth, C. T. Kresge, *Microporous Mesoporous Mater.* **144**, 158 (2011).
- S. Maheshwari *et al.*, *J. Am. Chem. Soc.* **130**, 1507 (2008).
- S. Maheshwari, thesis, University of Minnesota, Minneapolis, MN (2009).
- L. A. Nagahara, K. Hashimoto, A. Fujishima, D. Snowdenlfftt, P. B. Price, *J. Vac. Sci. Technol. B* **12**, 1694 (1994).
- P. Giannozzi *et al.*, *J. Phys. Condens. Matter* **21**, 395502 (2009).
- See SOM on Science Online.
- J. M. Cowley, A. F. Moodie, *Acta Crystallogr.* **10**, 609 (1957).
- E. J. Kirkland, R. F. Loane, J. Silcox, *Ultramicroscopy* **23**, 77 (1987).
- J. L. Schlenker, B. K. Peterson, *J. Appl. Cryst.* **29**, 178 (1996).
- The UDSKIP algorithm to calculate theoretical powder XRD patterns of ultra-small zeolite crystals is available at www.che.udel.edu/research_groups/nanomodelling/resources.html.
- P. Wu *et al.*, *J. Phys. Chem. B* **108**, 19126 (2004).
- S. Srivastava, N. A. Kotov, *Acc. Chem. Res.* **41**, 1831 (2008).
- M. Osada, T. Sasaki, *J. Mater. Chem.* **19**, 2503 (2009).
- J. Hedlund, F. Jareman, A. J. Bons, M. Anthonis, *J. Membr. Sci.* **222**, 163 (2003).
- P. S. Lee *et al.*, *J. Am. Chem. Soc.* **133**, 493 (2011).
- Z. P. Lai *et al.*, *Science* **300**, 456 (2003).
- J. Caro, M. Noack, *Microporous Mesoporous Mater.* **115**, 215 (2008).
- J. Choi *et al.*, *Science* **325**, 590 (2009).

Acknowledgments: We acknowledge support from the U.S. Department of Energy (DOE) (grant DE-09FE0001322), the Petroleum Institute of Abu Dhabi through the ADMIRE partnership, NSF (grant NSF-NIRT CMMI 0707610), and the Industrial Partnership for Research in Interfacial Materials and Engineering and Minnesota Supercomputing Institute at the University of Minnesota. Aspects of this work (MFI nanosheet synthesis and imaging by TEM) were supported as part of the Catalysis Center for Energy Innovation, an Energy Frontier Research Center funded by DOE's Office of Science, Office of Basic Energy Sciences under Award Number DESC0001004. Portions of it were conducted at the University of Minnesota Characterization Facility, which receives partial support from NSF through the National Nanotechnology Infrastructure Network.

Supporting Online Material

www.sciencemag.org/cgi/content/full/334/6052/72/DC1
Materials and Methods
SOM Text
Figs. S1 to S12
References (35–44)

25 May 2011; accepted 29 July 2011
10.1126/science.1208891

A Major Constituent of Brown Algae for Use in High-Capacity Li-Ion Batteries

Igor Kovalenko,¹ Bogdan Zdyrko,² Alexandre Magasinski,¹ Benjamin Hertzberg,¹ Zoran Milicev,¹ Ruslan Burtovyy,² Igor Luzinov,^{2*} Gleb Yushin^{1*}

The identification of similarities in the material requirements for applications of interest and those of living organisms provides opportunities to use renewable natural resources to develop better materials and design better devices. In our work, we harness this strategy to build high-capacity silicon (Si) nanopowder-based lithium (Li)-ion batteries with improved performance characteristics. Si offers more than one order of magnitude higher capacity than graphite, but it exhibits dramatic volume changes during electrochemical alloying and de-alloying with Li, which typically leads to rapid anode degradation. We show that mixing Si nanopowder with alginate, a natural polysaccharide extracted from brown algae, yields a stable battery anode possessing reversible capacity eight times higher than that of the state-of-the-art graphitic anodes.

A typical procedure for the preparation of Li-ion battery electrodes includes mixing electroactive powder with conductive carbon additives and a polymeric binder dissolved in a solvent. The produced slurry is then cast on metal foil current collectors and dried. Traditionally, most research has been focused

on synthesis of active powders with improved properties, and less attention was devoted to the advancement of the electrically inactive components of battery electrodes, such as binders. Yet recent studies have shown that many important battery characteristics, including stability and irreversible capacity losses, are critically dependent on the binder's properties (1–4). High-capacity electrochemically active particles that exhibit substantial volume changes during insertion and extraction of Li require improved binder characteristics to ensure electrode integrity during use. Si, in particular, exhibits the largest volume changes during Li-ion battery operation. The in-

terest in Si-based anodes (1, 5–11) stems from the abundance of Si in nature, its low cost, and its high theoretical capacity, which is an order of magnitude higher than that of the conventionally used graphite.

Recent studies have shown that synthetic and bio-derived polymers that contain carboxy groups, such as polyacrylic acid (PAA) and carboxymethyl cellulose (CMC), demonstrate promising characteristics as binders for Si-based anodes (1, 9, 12). Low binder extensibility did not demonstrate a negative effect on the battery performance (12). Reasonably stable anode performance, however, could only be achieved when Si volume changes were minimized by incomplete Li insertion in the tests (9) or accommodated by the use of extra-large binder content (1, 13), which lowers the resulting anode capacity. The polar hydrogen bonds between the carboxy groups of the binder and the SiO₂ on the Si surface were proposed to exhibit a self-healing effect and reform if locally broken (1). An alternative explanation for the observed stability of the rigid binders with lower extensibility could be that Si nanoparticles deform plastically during electrochemical alloying with Li (8), expanding toward the existing pores between the particles.

Here, we report that alginate, a high-modulus natural polysaccharide extracted from brown algae, yields a remarkably stable battery anode. Unlike many polysaccharides commonly found

¹School of Materials Science and Engineering, Georgia Institute of Technology, Atlanta, GA 30332, USA. ²School of Material Science and Engineering and Center for Optical Materials Science and Engineering Technologies, Clemson University, Clemson, SC 29634, USA.

*To whom correspondence should be addressed. E-mail: luzinov@clemson.edu (I.L.); yushin@gatech.edu (G.Y.)

in terrestrial plants, alginates, a major constituent of brown algae (Fig. 1A) and many aquatic microorganisms, contain carboxylic groups in each of the polymer's monomeric units (Fig. 1A). A higher content of carboxylic group in the binder should lead to a larger number of possible binder-Si bonds and, thus, better Si electrode stability (1). The extraction of alginates (commonly in a Na salt form) from algae proceeds by heating algae in a hot soda (Na_2CO_3) solution, which results in the dissolution of its alginate component. From a chemical standpoint, alginate (also called alginic acid) is a copolymer of 1→4 linked β -D-mannuronic acid (M) and α -L-guluronic acid (G) residues (Fig. 1A). Different compositions and sequences of M and G monoblocks in alginates yield a plethora of physical and biological properties, optimized in brown algae for a given environment. For example, algae growing in coastal areas have higher G content than the same algae growing in streaming waters (14). A high content of G makes alginate gels more rigid (14). Multivalent ions from seawater can cross-link the matrix, also increasing the rigidity of the plant body (15).

The ratio of M-to-G monoblocks in alginates may range from 0.3 to 9, with a typical value in commercial samples being ~1 (16). Nuclear magnetic resonance (NMR) spectroscopy measurements (Fig. 1B) revealed that the ratio of M-to-G monoblocks in the Na alginate sample used in this study was 1.13. This ratio was calculated on the basis of integration of the peaks at 4.7, 5.3, and 5.7 parts per million (Fig. 1B). Atomic force microscopy indentation studies showed that in a dry state, films made of the Na alginate exhibited ~6.7 times higher stiffness than dry films of polyvinylidene difluoride (PVDF), a common commercial binder used in Li-ion battery electrodes (Fig. 1, C and E). Interestingly, when immersed into the electrolyte solvent, the stiffness of alginate did not change appreciably (Fig. 1D), whereas the PVDF films became nearly 50 times softer (Fig. 1F). Ellipsometry studies show no detectable swelling of thin (~70-nm) Na-alginate films in the electrolyte solvent vapors. In contrast, PVDF films of similar thickness attract substantial amounts of carbonates from the vapor, demonstrating changes in thicknesses of ~20%. The negligibly small swellability of the alginate indicates a low level of polymer/electrolyte interaction. This property may prevent undesirable access of the electrolyte liquid to the binder/Si interface. The similar behavior of Na-CMC binders (fig. S1) probably explains their promising performance with Si anodes as well (1, 9, 17).

Scanning electron microscopy (SEM) studies showed the majority of Si nanoparticles used in our studies to be of elliptical or spherical shape with diameter in the range of 20 to 100 nm (fig. S2A). X-ray diffraction (XRD) (fig. S2B) studies revealed no impurities in the nanopowder. The average Si crystal size was calculated from the XRD data to be ~37 nm. The shape of the N_2 adsorption/desorption isotherms collected on

the Si nanopowder (type II, according to the Brunauer classification) is typical for macroporous (>50-nm) solids with unrestricted multi-layer adsorption (fig. S2C). The specific surface area of the Si nanopowder calculated with the Brunauer-Emmett-Teller equation is $96 \text{ m}^2/\text{g}$, which is much higher than 0.5 to $10 \text{ m}^2/\text{g}$ found in graphites used in Li-ion batteries. Assuming the density of Si nanoparticles to be $2.3 \text{ g}/\text{cm}^3$, the average Si particle size can be calculated to be ~27 nm, which is close to what we observed with SEM and estimated using XRD measure-

ments. The electrodes prepared using Si nanopowder, conductive C additives, and Na-alginate show a uniform structure and a smooth surface (fig. S2D) with small (<100-nm) pores visible between the nanoparticles. We estimated the electrode density to be $0.50 \text{ g}/\text{cm}^3$. Assuming the theoretical density of graphite, Si, and alginate to be accurate, one can estimate the remaining pore volume of the electrode to be ~five times the volume of Si particles. In recent studies on electrochemical alloying of Si in a nanoconfined space, we demonstrated that nano-Si may undergo the

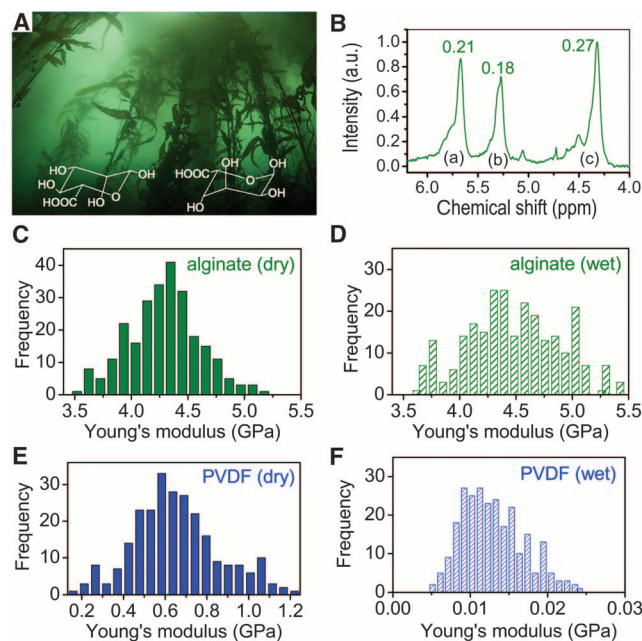


Fig. 1. Alginate origin and characterization. (A) Giant kelp forest (*Macrocystis pyrifera* algae) in the Pacific Ocean, photographed near the coast of California, USA. The insets show the chemical structure of mannuronic (left) and guluronic (right) acids. (B) ^1H NMR spectrum of Na-alginate. The numbers above the peaks marked as (a), (b), and (c) correspond to their integrated intensities. ppm, parts per million; a.u., arbitrary units. (C to F) Comparison between Young's modulus of Na-alginate and PVDF and in a dry [(C) and (E)] and wet [impregnated with electrolyte solvent, (D) and (F)] state.

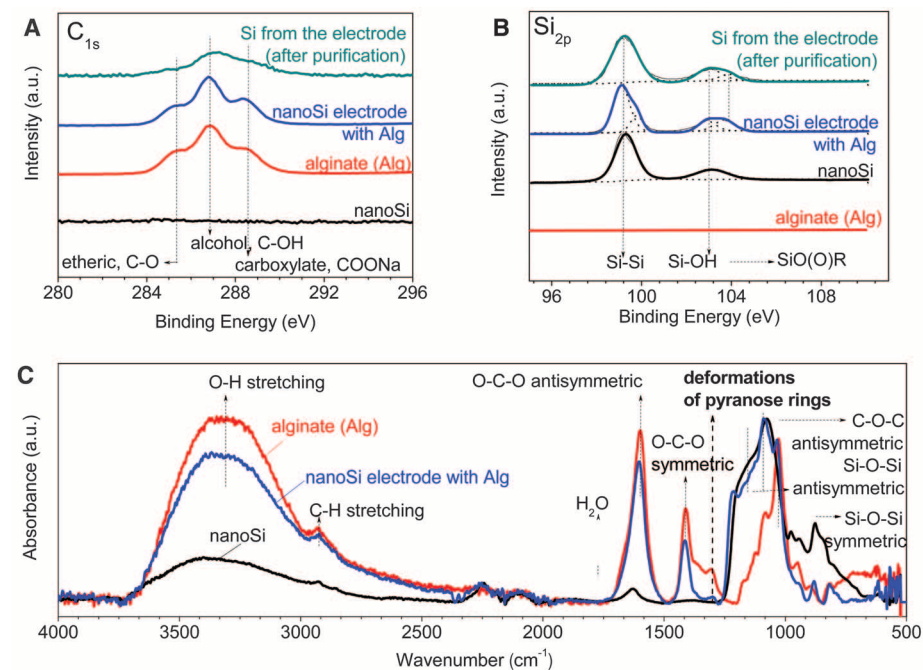


Fig. 2. Spectroscopic characterization of the nano-Si Na-alginate and electrodes prepared by mixing nano-Si with Na-alginate binder. (A and B) XPS spectra of alginate, Si nanopowder, nano-Si electrode, and Si nanopowder extracted from the electrode after extensive purification. (C) FTIR spectra of alginate, Si nanopowder, and nano-Si electrode.

irreversible shape changes upon the initial Li insertion, adapting to the restricted shape of the rigid pore (8). In subsequent cycles, however, the Si-Li alloy may exhibit fully reversible shape changes (8). Therefore, even if the rigidity of the alginate binder would prevent electrode expansion upon the first Li insertion, the initial electrode porosity could offer space to accommodate the volume changes in Si during cycling.

To evaluate the interactions of Na-alginate with Si and C particles, we have prepared electrodes consisting of pure Si/alginate and pure C/alginate mixtures. After drying the electrodes in vacuum (0.01 Torr) at 105°C for 4 hours, we have immersed pieces of the electrodes in large beakers filled with deionized (DI) water (alginate solvent) and stirred for 4 hours. After filtering and drying in air, the Si (or C) particles were collected, immersed in DI water, stirred for 4 hours, and filtered. We repeated this procedure five times. Before spectroscopy measurements, all samples were dried in a vacuum at 105°C for at least 8 hours. The C_{1s} core-level x-ray photoelectron spectroscopy (XPS) spectra of the alginate and Si-alginate films show three characteristic peaks corresponding to ether, hydroxyl, and carboxylate functional groups (Fig. 2A). As expected, the initial Si powder does not show any signs of C atoms on the surface. In spite of the extensive purification of the Si powder after mixing with alginate, the powder retains substantial content of alginate residues on the surface (Fig. 2A, top). A comparison of the C_{1s} spectra of DI water-cleaned Si nanopowder before and after mixing with Na-

alginate suggests formation of strong hydrogen bonding between the hydroxylated Si surface and alginate carboxylic moieties. Somewhat similar conclusions could be made by analyzing the Si_{2p} core-level peaks. Before mixing with alginate, the Si nanopowder surface shows a strong bulk Si peak at ~99.2 eV and a peak corresponding to hydroxyl functional groups at ~103 eV (Fig. 2B). However, an additional peak corresponding to R(O)-O-Si at 103.9 eV (9) is observed after mixing Si with Na-alginate and vacuum annealing to form an electrode (Fig. 2B). This peak is mostly retained after the extensive cleaning of the Si nanopowder described above (Fig. 2B, top). Analogous XPS experiments with C additives (fig. S3) suggest rather similar interactions between the polar groups and defects on the carbon surface and alginate moieties.

Fourier transform infrared (FTIR) spectroscopy studies provide further support for the strong bonding between the alginate and Si powder. A Na-alginate film exhibits a broad absorption band at ~3320 cm^{-1} related to hydrogen-bonded O-H stretching vibrations, a peak at ~1598 cm^{-1} corresponding to O-C-O (carboxylate) asymmetric vibrations, a peak at ~1410 cm^{-1} corresponding to O-C-O symmetric vibrations, a peak at ~1300 cm^{-1} related to the C-C-H and O-C-H deformation of pyranose rings, and a peak at ~1028 cm^{-1} related to C-O-C asymmetric vibrations, among others (Fig. 2C) (18). After electrode formation, the relative intensity of the 1300 cm^{-1} peak related to pyranose-ring deformation vibrations decreases considerably when compared with pure

Na-alginate. This decrease provides evidence of a chemical interaction between the alginate and Si nanoparticles (19). The strong interactions between the binder and the Si surface have been previously identified as one of the most critical factors affecting the stability of Si-based electrodes (1, 9).

Coin cells with metallic Li counter electrode were employed to evaluate the electrochemical performance of all of the electrodes. In contrast to earlier studies on CMC binders, which often required low Si [33 weight percent (wt %)] and high binder and carbon-additive (33 wt % each) content (1, 13), we used a high ratio of Si to C (Si:C = 3:1) and a considerably smaller amount of binder (15 wt %) for our tests.

Charge-discharge cycling performed with Li insertion capacity limited to 1200 mA·hour/g Si showed stable anode performance for more than 1300 cycles (Fig. 3A). In real-life applications, however, a noticeable variation in the degree of lithiation of individual Si particles may take place. Therefore, it is important to test the ability of Si anodes and Si-binder interface to withstand the largest volume changes taking place during full lithiation. In our additional tests (Fig. 3, B to D, and fig. S4), we inserted Li to nearly 100% depth of discharge (to 0.01 mV versus Li/Li⁺) and additionally held the anode at this potential for more than 10 min. Because the average time of full Li insertion into 100-nm diameter Si nanoparticles is 6 min (20) and average Si particles in our electrode are only 27 nm, this procedure warranted that a large portion of the Si particles (close to a Cu foil) be fully lithiated. In spite of the severe testing conditions, an alginate binder allowed for a stable performance of Si electrodes (Fig. 3B and fig. S4). This is in contrast to Si anodes with PVDF and Na-CMC, which demonstrated poor stability (Fig. 3B). At a current density of 4200 mA/g, the reversible Li extraction specific capacity of an alginate-based Si anode is in the range of 1700 to 2000 mA·hour/g (Fig. 3, B and C, and fig. S4), which is ~five times higher than the theoretical capacity of graphite and 9 to 23 times higher than the experimentally determined capacity of graphites (85 to 190 mA·hour/g) at such a high current density. At a smaller current density of 140 mA/g (Fig. 3C and fig. S4), the specific capacity of the Si anode reaches 3040 mA·hour/g, which is more than 8 times higher than the theoretical specific capacity of graphite (372 mA·hour/g). The contribution of Si nanopowder alone could be calculated as ~4000 mA·hour/g, which is consistent with observations on other nano-Si materials (1, 7, 8) but is noticeably higher than what was previously observed for micron-size Si (21). The volumetric anode capacity was determined to be ~1520 mA·hour/cm³ at 140 mA/g current density, which is 2.5 times higher than ~620 mA·hour/cm³ for graphitic anodes.

We propose that a stable binder for Si anodes needs to possess several critical properties. First, a very weak binder-electrolyte interaction is needed for the long-term anode stability. All of the binders

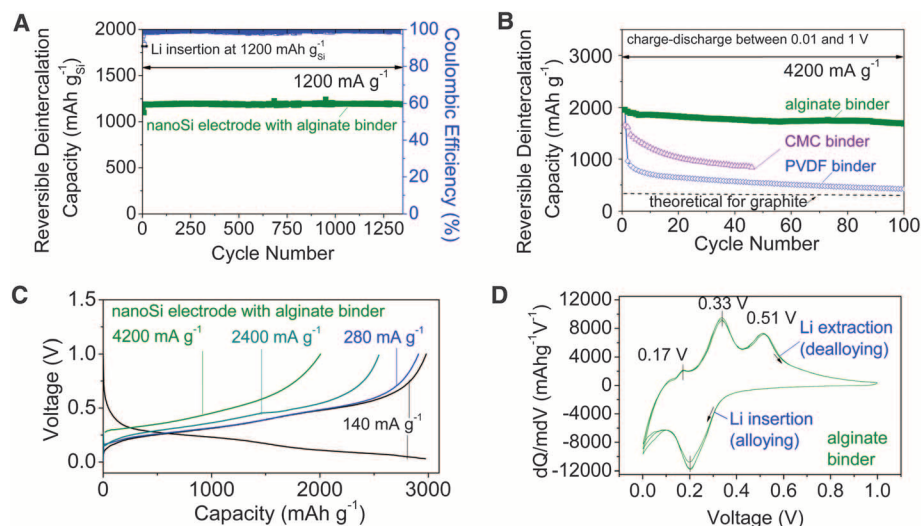


Fig. 3. Electrochemical performance of alginate-based nano-Si electrodes (electrode density = 0.50 g/cm³, weight ratio of Si:C = 3:1). (A) Reversible Li-extraction capacity and CE of the nano-Si electrodes versus cycle number for Li insertion level fixed to 1200 mA·hour/g Si (Ah, ampere hour). (B) Reversible Li-extraction capacity of nano-Si electrodes with alginate, CMC, and PVDF binders versus cycle number collected for the current density of 4200 mA/g for cells cycled in the potential window of 0.01 to 1 V versus Li/Li⁺. (C) Galvanostatic discharge profiles of the nano-Si electrode at different current densities between 0 and 1 V. (D) Differential capacity curves of the nano-Si electrode in the potential window of 0 to 1 V versus Li/Li⁺ collected at the rate of 0.025 mV/s after the first galvanostatic charge-discharge cycle. Q/m, specific capacity; V, voltage. All electrochemical measurements were performed at room temperature in two-electrode 2016 coin-type half-cells. In (A), the capacity is reported for the Si contribution only. In (B) to (D), the capacity is normalized by the total weight of Si and C additives.

that provide at least satisfactory performance in Si anodes (including CMC and PAA) experience virtually no swelling in commonly used electrolytes (Fig. 1 and fig. S1) (12). If a solvent reaches the Si electrode surface by permeating through a binder layer, it decomposes (22–24). The solvent-decomposition products deposited in the region between the binder and the Si would substantially weaken the Si-binder bond strength and lead to rapid anode degradation (PVDF in Fig. 3B). Therefore, little-to-no interaction between the binder and the solvent is needed to prevent access of the solvent molecules to the Si-binder boundary.

Another property of an ideal Si binder is to provide access of Li ions to the Si surface. Therefore, if a binder is not permeable to solvent electrolyte molecules, it should either cover only a portion of the Si surface or remain permeable to Li ions. Due to the small size of Si nanopowder and its resultant high surface curvature, the number of anchor points between binder polymeric chains and Si particles is limited, suggesting that a portion of the Si surface should indeed be directly exposed to the electrolyte. Our XPS studies on alginate-coated Si particles show that a portion of Si surface is alginate-free (Fig. 2B). To identify the conductivity of Li-ions through Na-alginate, we deposited a thin (1- μm) layer on Cu foil and performed cyclic voltammetry and electrochemical-impedance spectroscopy tests with Li foil as a counter electrode (fig. S5). Both tests revealed small but sufficient ionic conductance. From the impedance data, we determined the Warburg constant and estimated the diffusion coefficient of Li in Na-alginate to be $\sim 10^{-8}$ S/cm. Although this is four orders of magnitude smaller than the diffusion coefficient of Li in solid electrolytes (25), the nanometer-level thickness of a Na-alginate layer compensates for its limited diffusivity. The proposed mechanism of ion transport through the alginate film is via hopping of Li ions between the adjacent carboxylic sites, similarly to alginate's function for the ion transport in the algae cells (15).

Third, an ideal binder should assist in building a deformable and stable solid-electrolyte interphase (SEI) on the Si surface. High Coulombic efficiency (CE) is critical for practical applications and is challenging to achieve in Si-based

anodes because of the need to maintain a stable SEI layer, in spite of the large changes in particle volume (and, therefore, surface area) during the battery operation. In ultrathin Si films, high stability is achieved (26) because the film surface area does not change during cycling, and the volume changes are accommodated largely via variation in film thickness. Thus, maintaining a stable SEI is not a challenge. In thicker films that exhibit cracks at the current collector-Si interface and, thus, experience some surface-area changes, electrolyte additives are needed to achieve a stable SEI. In free-standing Si nanowires that do not need a binder but experience much more substantial surface-area changes upon cycling, the unprotected Si fails to maintain a stable SEI, causing continuous Li consumption, increasing Si surface roughness, and decreasing CE with every cycle (27). Si nanowires commonly demonstrate CE of only 93 to 97% (5). In contrast, our electrodes show improving CE with every cycle approaching 99.9% (fig. S4A), suggesting that the alginate binder contributes to building a stable passivating SEI layer. To test our hypothesis that Na-alginate assists in building a stable SEI, we performed XPS studies on our electrodes before and after cycling (Fig. 4). The surface chemistry of the SEI did not noticeably change between the 10th and 200th cycle, suggesting excellent SEI stability and fully supporting our hypothesis. Earlier studies performed on graphitic anodes also suggested that interactions between the functional groups of Na-CMC and electrolyte may contribute to the SEI formation and explain Na-CMC's good performance (28). Its positive impact on improving CE of Si anodes was observed as well (1), but only when the relative amount of Na-CMC was several times higher than that of Na-alginate (13). The complex interactions between Na cations, Si, and various electrolytes deserve a separate study.

Even if the stability of the SEI and binder-Si interface is achieved, binders that show low extensibility under stress require the Si electrode to possess sufficient pore volume, which is needed for Si expansion. Increasing the pore volume of CMC-based Si electrodes markedly improved their stability (29). The lack of sufficient pore volume may cause sealing of the interparticle

pores (and, thus, a dramatic reduction in the ion transport) and mechanical failure of the electrode during operation. The smallest sufficient pore volume should be larger than the total volume of Si expansion for several reasons. First, the shape of the Si particles and the shape of the pores are different. Therefore, at the fully expanded state some pore volume will remain unfilled. Note that plastic deformation of lithiated Si nanoparticles may take place (8), thereby reducing the strictness of the requirements on local pore shape and size. However, strong bonding of the binder to Si particles (Fig. 2) and high binder stiffness (Fig. 1D) is needed, because the endurance limit of the binder and the binder-Si interface must exceed the internal stresses in the electrode caused by the volume expansion of Si nanoparticles. Second, the SEI formation requires some available volume as well. Furthermore, at the expanded state Si particles could be pressed against each other, inducing highly undesirable damage in the SEI. Finally, open pores not filled with any electrolyte decomposition products are needed for the rapid transport of Li ions within the electrode. Too large a pore volume, however, will lead to a decrease in the volumetric capacity of the anode. Because the considerations discussed above make it difficult to precisely predict the minimum pore volume, we performed additional experiments to intentionally densify our electrodes. We noticed that when the electrode density was increased to ~ 0.75 g/cm³ (and the total pore volume equal to 2.7 times the volume occupied by Si particles), the electrodes showed noticeably worse performance (fig. S6). Therefore, we estimate that the ideal pore volume should be somewhere between three and six times the volume of Si component of the electrode, provided that the binder has properties similar to that of alginate or CMC.

Because both CMC and alginate exhibit similar mechanical properties (Fig. 1, C and D, and fig. S1, A and B) and show no interaction with electrolyte, we conclude that the differences in their chemical properties explain the considerable difference in their performance in Si electrodes of similar porosity levels (Fig. 3B). In alginate, carboxylic groups are naturally present and evenly distributed in the polymer chain, whereas in CMC they are synthetically induced and their

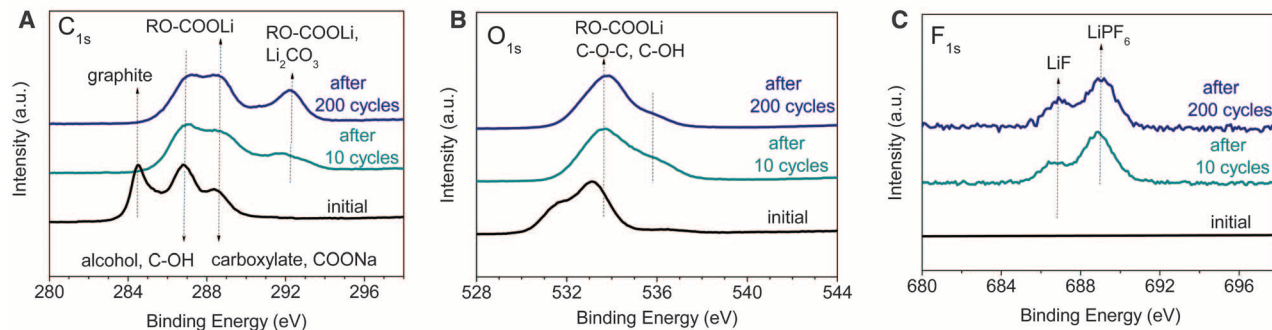


Fig. 4. Stability of the SEI layer in an alginate-based Si anode. (A to C) XPS spectra on the anode surface before and after cycling in the potential range 0.01 to 1 V versus Li/Li⁺. No major changes in the chemistry of the SEI of the anode cycled for 10 or 200 cycles are visible.

distribution is random, where some monomeric units may have more than one carboxylic group and other have none. The higher concentration and a more uniform distribution of the carboxylic groups along the chain in alginate (Fig. 1A) could be responsible for the better transport of Li ions in the vicinity of Si particles, more uniform coverage, and more efficient assistance in the formation of a stable SEI layer on the Si surface (Fig. 4). Alginate macromolecules are also much more polar than the CMC polymer chains, which can ensure better interfacial interaction between the polymer binder and the particles, as well as stronger adhesion between the electrode layer and Cu substrate. This large difference in chemistry of CMC and alginate results in major differences in their behavior. For example, the alginate solution in water has dramatically higher viscosity than CMC (fig. S7). This high viscosity prevents Si particles from sedimentation and aggregation during the electrode formation, as water is evaporating, resulting in high slurry uniformity. This uniformity is known to be critical for obtaining uniform distribution of active materials within the anode needed for the long-term electrode stability. Alginate solution also exhibits a much higher degree of shear-thinning behavior (fig. S8), which offers an opportunity to lower a slurry viscosity needed for fast homogenization by increasing the mixing rate and an opportunity to increase a slurry viscosity for porosity and uniformity control during the electrode formation by lowering the mixing rate. To achieve viscosity comparable to alginate solutions, substantially higher CMC content is needed. Similarly, to get a remotely comparable performance with a CMC binder, one needs to increase the binder:Si ratio by a factor of 4 (1, 13). The high binder content decreases the electrical conductivity of the electrode and necessitates the use of a higher content of the conductive carbon additives (increasing the C:Si ratio by a factor of 3) (1), which inevitably lowers the electrode specific capacity.

To further characterize the behavior of the alginate-based electrode, we performed cyclic voltammetry experiments. The differential capacity curves show one broad Li insertion (cathodic) peak at ~ 0.21 V and two Li extraction (anodic) peaks at 0.33 and 0.51 V (Fig. 3D). The origin of the potential difference between the corresponding peaks in the cathodic and anodic directions is commonly modeled by a thermodynamic (rate-independent) hysteresis (30). The first 0.33-V anodic peak is not always observed. In some Si-C nanocomposite particles, for example, only one Li extraction peak at ~ 0.5 V appears (6). Therefore, the 0.33-V peak could be related to the surface properties of Si. A small Li-extraction peak observed at ~ 0.17 V corresponds to Li deintercalation from C additives. The five cyclic voltammetry cycles (Fig. 3D) demonstrate high reproducibility, indicative of good anode stability.

The shapes of the galvanostatic Li insertion and extraction profiles for the produced Si anodes

(Fig. 3C and fig. S4B) are similar to the profiles previously reported in literature for other Si electrodes (6, 9, 13). In contrast to intercalation-type electrode materials, these profiles do not exhibit strictly horizontal plateaus and cover a larger potential range. The Li-extraction profiles become more horizontal and exhibit slightly smaller overpotential with cycling (fig. S4B), suggesting a gradual improvement in the discharge kinetics (20). The current-dependent overpotential increases the Li-extraction potential when current density is increased from 140 to 4200 mA/g (20) (Fig. 3C). By comparing the Li-extraction capacities achieved at different current densities (Fig. 3C), we can conclude that these electrodes possess moderate rate capability, inferior to that achieved in Si-C composite anodes with hierarchical porosity (6) or in nanowires (5, 10). The advantage of this traditional battery technology, however, is higher volumetric capacity, higher CE, and compatibility with existing manufacturing techniques. Further electrode optimization and introduction of additional pores is expected to substantially increase the rate performance, because the diffusion of Li into or out of Si nanoparticles can be achieved within minutes (20).

In addition to improving performance of Si anodes, the alginate properties may provide advantages to other electrodes, such as traditional graphitic anodes. For example, replacing PVDF with lower-cost, environmentally friendly alginate was found to improve the first-cycle CE and cycle stability (fig. S9).

References and Notes

1. J. S. Bridel, T. Azais, M. Morcrette, J. M. Tarascon, D. Larcher, *Chem. Mater.* **22**, 1229 (2010).
2. L. Fransson, T. Eriksson, K. Edstrom, T. Gustafsson, J. O. Thomas, *J. Power Sources* **101**, 1 (2001).
3. S. S. Zhang, T. R. Jow, *J. Power Sources* **109**, 422 (2002).
4. D. Guy, B. Lestriez, D. Guyomard, *Adv. Mater.* **16**, 553 (2004).
5. C. K. Chan *et al.*, *Nat. Nanotechnol.* **3**, 31 (2008).
6. A. Magasinski *et al.*, *Nat. Mater.* **9**, 353 (2010).

7. K. Kang *et al.*, *Appl. Phys. Lett.* **96**, 053110 (2010).
8. B. Hertzberg, A. Alexeev, G. Yushin, *J. Am. Chem. Soc.* **132**, 8548 (2010).
9. D. Mazouzi, B. Lestriez, L. Roue, D. Guyomard, *Electrochem. Solid-State Lett.* **12**, A215 (2009).
10. H. Kim, J. Cho, *Nano Lett.* **8**, 3688 (2008).
11. M. H. Park *et al.*, *Nano Lett.* **9**, 3844 (2009).
12. A. Magasinski *et al.*, *ACS Appl. Mater. Interfaces* **2**, 3004 (2010).
13. S. D. Beattie, D. Larcher, M. Morcrette, B. Simon, J. M. Tarascon, *J. Electrochem. Soc.* **155**, A158 (2008).
14. O. Smidsrod, K. I. Draget, *Carbohydr. Eur.* **14**, 6 (1996).
15. A. J. de Kerchove, M. Elimelech, *Biomacromolecules* **8**, 113 (2007).
16. K. I. Draget, G. Skjåk-Braek, O. Smidsrod, *Int. J. Biol. Macromol.* **21**, 47 (1997).
17. J. Li, R. B. Lewis, J. R. Dahn, *Electrochem. Solid-State Lett.* **10**, A17 (2007).
18. T. A. Fenoradosa *et al.*, *J. Appl. Phys.* **22**, 131 (2010).
19. S. K. Papageorgiou *et al.*, *Carbohydr. Res.* **345**, 469 (2010).
20. R. Chandrasekaran, A. Magasinski, G. Yushin, T. F. Fuller, *J. Electrochem. Soc.* **157**, A1139 (2010).
21. M. N. Obrovac, L. Christensen, *Electrochem. Solid-State Lett.* **7**, A93 (2004).
22. E. Peled, D. Golodnitsky, G. Ardel, V. Eshkenazy, *Electrochim. Acta* **40**, 2197 (1995).
23. D. Aurbach, *J. Power Sources* **89**, 206 (2000).
24. J. B. Goodenough, Y. Kim, *Chem. Mater.* **22**, 587 (2010).
25. Z. Gadjourva, Y. G. Andreev, D. P. Tunstall, P. G. Bruce, *Nature* **412**, 520 (2001).
26. S. Ohara, J. Suzuki, K. Sekine, T. Takamura, *J. Power Sources* **136**, 303 (2004).
27. J. W. Choi *et al.*, *Nano Lett.* **10**, 1409 (2010).
28. L. El Ouatani *et al.*, *J. Power Sources* **189**, 72 (2009).
29. J. C. Guo, C. S. Wang, *Chem. Commun.* **46**, 1428 (2010).
30. M. D. Levi, D. Aurbach, *J. Phys. Chem. B* **101**, 4630 (1997).

Acknowledgments: This work was partially supported by Georgia Institute of Technology, Honda Initiation Grant, Clemson Univ., and NASA grant NNX09CD29P. Patent application PCT US 113507 has been filed.

Supporting Online Material

www.sciencemag.org/cgi/content/full/science.1209150/DC1
Material and Methods
Figs. S1 to S9

31 May 2011; accepted 19 August 2011
Published online 8 September 2011;
10.1126/science.1209150

A Self-Quenched Defect Glass in a Colloid-Nematic Liquid Crystal Composite

T. A. Wood, J. S. Lintuvuori, A. B. Schofield, D. Marenduzzo, W. C. K. Poon*

Colloidal particles immersed in liquid crystals frustrate orientational order. This generates defect lines known as disclinations. At the core of these defects, the orientational order drops sharply. We have discovered a class of soft solids, with shear moduli up to 10^4 pascals, containing high concentrations of colloidal particles (volume fraction $\phi \geq 20\%$) directly dispersed into a nematic liquid crystal. Confocal microscopy and computer simulations show that the mechanical strength derives from a percolated network of defect lines entangled with the particles in three dimensions. Such a "self-quenched glass" of defect lines and particles can be considered a self-organized analog of the "vortex glass" state in type II superconductors.

In a typical colloidal suspension, particles are dispersed in a simple, isotropic liquid that acts as a passive, homogeneous background

medium. But it is also possible to disperse particles in a liquid that itself has complex properties. For example, particles in a demixing binary